Absorption and Fluorescence Lineshape Theory for Polynomial Potentials

JCTC Journal of Chemical Theory and Computation

Article

Absorption and Fluorescence Lineshape Theory for Polynomial Potentials

André Anda, Luca De Vico, Thorsten Hansen, and Darius Abramavicius

J. Chem. Theory Comput., **Just Accepted Manuscript** • DOI: 10.1021/acs.jctc.6b00997 • Publication Date (Web): 19 Oct 2016

ACS Publications

Journal of Chemical Theory and Computation is published by the American Chemical Society. 1155 Sixteenth Street N.W., Washington, DC 20036

Absorption and Fluorescence Lineshape Theory for Polynomial Potentials

André Anda,*,† Luca De Vico,† Thorsten Hansen,† and Darius Abramavičius‡

Department of Chemistry, University of Copenhagen, Universitetsparken 5, DK-2100, København Ø, Denmark , and Department of Theoretical Physics, Faculty of Physics, Sauletekio ave. 9, Build. 3, LT-10222 Vilnius, Lithuania

E-mail: andre@chem.ku.dk

Abstract

The modelling of vibrations in optical spectra rely heavily on the simplifications brought about by using harmonic oscillators. Realistic molecular systems, however, can deviate substantially from this description. We develop two methods which show that the extension to arbitrarily shaped potential energy surfaces is not only straightforward, but also efficient. These methods are applied to an electronic two-level system with potential energy surfaces of polynomial form, and used to study anharmonic features such as the zero-phonon line shape and mirror symmetry breaking between absorption and fluorescence spectra. The first method, which constructs vibrational wavefunctions as linear combinations of the harmonic oscillator wavefunctions, is shown to be extremely robust and can handle large anharmonicities. The second method uses the cumulant expansion which is readily solved even at high orders, thanks to an ideally suited matrix theorem.

*To whom correspondence should be addressed

†Department of Chemistry, University of Copenhagen, Universitetsparken 5, DK-2100, København Ø, Denmark

‡Department of Theoretical Physics, Faculty of Physics, Sauletekio ave. 9, Build. 3, LT-10222 Vilnius, Lithuania

Introduction

The interplay of electronic and vibrational motion is normally associated with relaxation and dephasing mechanisms, but has also been suggested to play a constructive role in energy transfer and charge separation in photosynthesis.[1,2] All of these phenomena are studied with optical experiments which induce simultaneous transitions between electronic and vibrational states. Combining the experimental data with theoretical models can reveal the energetics of the molecular system and in turn the underlying physics of the abovementioned processes.

At room temperature, spectral features are broadened by the thermal energy, making it difficult to discern the vibrational structure. By cooling the system down, individual peaks corresponding to particular transitions in the system emerge. The zero phonon line (ZPL) originating from purely electronic transitions is normally a dominant feature in the spectrum, while concurrent electronic and vibrational transitions form the phonon side band, which is directly measurable in low-temperature delta-fluorescence line narrowing experiments.[3] Recent theoretical work has demonstrated the potential of low-temperature two-dimensional electronic spectroscopy to reveal more detailed and altogether new insight into the electronic-vibrational couplings.[4]

However, the vibrational content may depend on the electronic configuration. This is due to anharmonicities. The standard theoretical models come short at this level of detail, since they draw heavily on the simplifications brought about by using harmonic oscillators. These simplifications include well-known wavefunctions, evenly spaced energy levels and linear coupling between electronic and vibrational states, leading to exact truncation of the cumulant expansion at second order in the energy gap fluctuation operator. Although it is often an excellent approximation, realistic molecular oscillators are never perfectly harmonic. The simple case of the diatomic molecule is well-known to be better described by the Morse potential, $V_{Morse}(x) = D[1 - e^{-\alpha(x-x_{eq})}]^2$, which ensures a high repulsion energy at short distances and also that the molecule dissociates at long distances. Here, D is the depth of the potential, α is the width and x_{eq} is the equilibrium position. But also highly complex

biomolecules such as the light-harvesting complex LH2 in purple bacteria exhibit strong anharmonic behaviour.[5] Other oscillators, such as the proton in a hydrogen bond, may take on a range of qualitatively different shapes, including double-well and quartic potentials.[6,7] For these systems it is dubious to model vibrations as harmonic oscillators.

By going beyond the harmonic approximation, the system evolution is characterised by non-Gaussian dynamics. The effect of non-Gaussian fluctuations on spectroscopic observables has previously been studied using molecular dynamics simulations[8–10] and stochastic environments,[11–13] but in our work we will include anharmonic potentials in the system Hamiltonian.

Early work[14–20] on modelling anharmonic oscillators, pioneered by Osad'ko, Skinner and Hsu, used quadratic coupling terms, and maintained analytical expressions for the response functions. More recent work in this vein is presented in a paper by Fidler and Engel.[21] However, here the cumulant expansion is truncated at third order, permitting only an approximate solution for the response functions. Tanimura and Okumura[22] found analytical expressions for the first-, third- and fifth-order response functions for displaced anharmonic oscillators, using the Liouville-space generating functional, but were limited to quite small perturbations from the harmonic potential. Jansen and Mukamel derived closed expressions for nonlinear response functions using an $\hbar$ expansion of the Liouville-space generating functional and correlation functions of collective coordinates.[23] Anharmonic features in the third order polarisation, obtained by 2D electronic spectroscopy, manifest as a curvature of the centre line of a peak.[24–26]

A quite different approach is to employ Morse oscillators. Tanimura and Maruyama[27] solved a hierarchy of Fokker-Planck equations of motion for three- and four-level systems of shifted Morse oscillators to obtain linear and nonlinear spectroscopic observables. Toutounji[28,29] used Morse coherent states to evaluate optical response functions. Here, the cumulant expansion was truncated at second order, neglecting possibly important higher order terms.

All of these methods have in common that they place severe restrictions on the shapes

of the surfaces. Moreover, a systematic improvement by including higher order cumulants or perturbations seems cumbersome. The work we present here will remedy both of these shortcomings. We will generalise the theory to an electronic two-level system with polynomial potential energy surfaces (PESs).

Of course, numerical methods exist for completely general PESs, most notably the multiconfiguration time-dependent Hartree method,[30,31] which is the state-of-the-art numerical method, specifically designed for multidimensionsal problems. For 1D potentials, the Numerov-Cooley method[32,33] is probably the best known. Lastly, Bytautas *et. al.*[34–36] calculate the vibration-rotation spectra of diatomic molecules by expanding the potential in even-tempered Gaussians and using the discrete variable representation[37] to solve the nuclear Schrödinger equation.

An important advantage of the methods developed in this paper, is the close connection to the various displaced harmonic oscillator models,[38–44] which are ubiquitous in physics and chemistry. We start by defining the model and proceed with the example of linear absorption and fluorescence. There are two common approaches to calculating these response functions, one which requires the energies and the wavefunctions to be known, and one where it is sufficient to define the ground and excited state Hamiltonians.

For the first approach, we find the energies using the method developed by Jafarpour and Afshar, which is summarised in appendix A. We then build upon this method to also find the vibrational wavefunctions as linear combinations of the harmonic oscillator wavefunctions, see appendix B.

For the second approach, we perform the cumulant expansion and derive a simple recursion relation for the cumulants. The evaluation of the cumulants is made extremely efficient using a matrix theorem.

Results are presented for the Morse oscillator and a generic anharmonic oscillator, with an ongoing discussion.

Model

The electronic two-level system we consider is governed by the following Hamiltonian:

$$H = H_g|g\rangle\langle g| + H_e|e\rangle\langle e| + H_{bath}, \tag{1}$$

where

$$H_g = \frac{p^2}{2m} + V_g(x), \tag{2}$$

$$H_e = \hbar\omega_{eg} + \frac{p^2}{2m} + V_e(x). \tag{3}$$

Here, p, x, m and $\hbar\omega_{eg}$ denote the momentum operator, the position operator, the reduced mass and the energy difference between the minima of the two electronic states, respectively. V_g and V_e are the ground and excited state potential energy surfaces which may have arbitrary shapes as long as they can be represented by polynomials, which essentially only excludes potentials that have cusps or discontinuities. H_{bath} describes the environment's degrees of freedom and their coupling to the two-level system. For a chromophore, these could be solvent fluctuations or intramolecular vibrations. The bath causes the remaining quantum system to dephase, which leads to line broadening in the absorption and fluorescence spectra. Since our focus is on the anharmonic features of the two-level system, we leave the bath Hamiltonian unspecified, but include its effect phenomenologically by multiplying optical response functions with an exponential decay function. In appendix E, we show how a more general dephasing mechanism can be implemented by formulating the cumulants in Liouville space. It should also be noted that, in principle, more elaborate models such as coupled two-level systems can also be treated with the same theory, but that is beyond the scope of this work.

Recall that the harmonic oscillator is described by

$$H_0 = \frac{p^2}{2m} + \frac{m\omega_0^2 x^2}{2}, \tag{4}$$

where ω_0 is the frequency of the oscillator. Introducing natural units by setting $\frac{\hbar^2}{m} = m\omega_0^2 = 1$, simplifies the equation to

$$H_0 = \frac{p^2}{2} + \frac{x^2}{2}, \tag{5}$$

where energy will be in units of $\hbar\omega_0$ and distance will be in units of $\sqrt{\frac{\hbar}{m\omega_0}}$. The ground and excited state Hamiltonians can now be defined as:

$$H_{g/e} = H_0 + \sum_{m=0}^{M} \lambda_m^{g/e} x^m. \tag{6}$$

Where the first anharmonic term is the third order term. The sum can be regarded as the perturbation potential with respect to the harmonic oscillator. It has been shown[45–47] that it is possible to calculate energy eigenvalues numerically for the quantum anharmonic oscillator when the Hamiltonian has this form. Although it is even possible to do this for N coupled quantum anharmonic oscillators[47] we restrict ourselves to the one-dimensional case.[46]

Lineshape Theory

Now that the two-level system is defined, we show how to calculate optical response functions. In the Condon approximation, the optical response functions are factorised into products of transition dipole moments, describing the strength of the electronic transition, and a lineshape function which describes the fine-structure resulting from vibrational transitions. For example, in linear absorption, the absorption coefficient is found as:

$$\alpha(\omega) \propto |\mu_{eg}|^2 \mathcal{D}_{abs}(\omega - \omega_{eg}), \tag{7}$$

where μ_{eg} is the transition dipole moment between the ground and excited state and $\mathcal{D}_{abs}$ is

the absorption lineshape function. Likewise, the fluorescence spectrum can be calculated as

$$I(\omega) \propto |\mu_{eg}|^2 \mathcal{D}_{flu}(\omega - \omega_{eg}), \tag{8}$$

where $\mathcal{D}_{flu}$ is the fluorescence lineshape function.

There are two standard approaches to calculating the lineshape functions,[48] each with pros and cons. In method 1, the lineshape functions are constructed by expanding the polarisation operator in electronic and vibrational eigenstates (complete diagonalisation). The vibrational energies and eigenfunctions are found using the methods in appendices A and B. The resulting expressions simply combine all possible Liouville space pathways with their amplitudes and evolution operators:

$$\mathcal{D}_{abs}(\omega - \omega_{eg}) = \frac{1}{2\pi\hbar} \sum_{M,N} \mathrm{Re} \int_0^\infty dt f_{gM} |\langle \chi_{gM} | \chi_{eN} \rangle|^2 e^{i\omega t - i(E_{eN} - E_{gM})t/\hbar - \gamma t}, \tag{9}$$

$$\mathcal{D}_{flu}(\omega - \omega_{eg}) = \frac{1}{2\pi\hbar} \sum_{M,N} \mathrm{Re} \int_0^\infty dt f_{eM} |\langle \chi_{eM} | \chi_{gN} \rangle|^2 e^{-i\omega t - i(E_{gN} - E_{eM})t/\hbar - \gamma t}, \tag{10}$$

where $\chi_{gM/eN}$ denote vibrational ground/excited states with corresponding energies $E_{gM/eN}$, $f_{aM} = \frac{e^{-E_{aM}/k_B T}}{\sum_m e^{-E_{am}/k_B T}}$ are the equilibrium ground/excited state occupations, where $a = \{g, e\}$, and $k_B T$ is the product of the Boltzmann constant and the temperature. $e^{-\gamma t}$ accounts phenomenologically for the bath-induced dephasing, with dephasing strength γ. Although eqs 9 and 10 are rather simple expressions, knowledge about the vibrational eigenstates in the system is often unattainable, especially for complex systems.

Alternatively, using method 2, one can calculate the lineshape functions directly from the Hamiltonian, without knowing the eigenfunctions and their energies. In this approach, the absorption lineshape function is given by

$$\mathcal{D}_{abs}(\omega - \omega_{eg}) = \frac{1}{2\pi\hbar} \mathrm{Re} \int_0^\infty dt \, \mathrm{Tr}\{S(t) \rho_g^{eq}\} e^{i(\omega - \omega_{eg})t - \gamma t}, \tag{11}$$

$$S(t) = T_+ \exp\left\{ -\frac{i}{\hbar}\int_0^t d\tau \Delta(\tau) \right\}, \tag{12}$$

$$\Delta(\tau) = e^{iH_g\tau}\Delta e^{-iH_g\tau}, \tag{13}$$

$$\Delta = H_e - H_g - \mathrm{Tr}\{(H_e - H_g)\rho_g^{eq}\}, \tag{14}$$

where $\rho_g^{eq} = \frac{e^{-H_g/k_BT}}{\mathrm{Tr}\, e^{-H_g/k_BT}}$ is the equilibrium density matrix of the vibrational states in the electronic ground state, T_+ is the positive time-ordering operator, and S is the evolution operator of Δ, the electronic energy gap fluctuation operator. This operator describes the deviation of the instantaneous electronic energy gap from its thermally averaged value. Again, the effect of the bath is accounted for by multiplying the response function by $e^{-\gamma t}$.

In complete analogy, we find the fluorescence lineshape function as

$$\mathcal{D}_{flu}(\omega - \omega_{eg}) = \frac{1}{2\pi\hbar}\,\mathrm{Re}\int_0^\infty dt\, \mathrm{Tr}\{\tilde{S}(t)\rho_e^{eq}\}e^{-i(\omega-\omega_{eg})t-\gamma t}, \tag{15}$$

$$\tilde{S}(t) = T_+ \exp\left\{ -\frac{i}{\hbar}\int_0^t d\tau \tilde{\Delta}(\tau) \right\}, \tag{16}$$

$$\tilde{\Delta}(\tau) = e^{iH_e\tau}\tilde{\Delta}e^{-iH_e\tau}, \tag{17}$$

$$\tilde{\Delta} = H_g - H_e - \mathrm{Tr}\{(H_g - H_e)\rho_e^{eq}\}, \tag{18}$$

where the inverse Fourier transform has been replaced by an ordinary Fourier transform and the gap has been defined relative to the excited state. The equilibrium density matrix is now calculated in the electronic excited state $\rho_e^{eq} = \frac{e^{-H_e/k_BT}}{\mathrm{Tr}\, e^{-H_e/k_BT}}$ and the dynamics is governed by the excited state Hamiltonian H_e.

The difficulty in solving the method 2 lineshape functions lies in the evaluation of the S and $\tilde{S}$ operators. Since S and $\tilde{S}$ are mathematically equivalent, we show how they can be calculated only for the absorption case.

The trace of an operator times the density matrix is just the expectation value, so we can write

$$\mathrm{Tr}\{S(t)\rho_g^{eq}\} = \langle S(t)\rangle. \tag{19}$$

To rewrite the expectation value of an exponential function into the an exponential function of expectation values, which is easier to work with, we employ the cumulant expansion,[49–52] which is exact in the infinite limit, but for practical purposes the series must be truncated. Here the properties of the harmonic oscillator are very useful as the series terminate at second order in Δ. Unfortunately, this does not hold for the anharmonic oscillator.[17] We then have to all orders:

$$\langle S(t)\rangle = \exp\left[\sum_{n=1}^{\infty} K_n(t)\right], \tag{20}$$

$$K_n(t) = (-i/\hbar)^n(1/n!)\int_0^t dt_1 \int_0^t dt_2 \cdots \int_0^t dt_n \langle T_+\Delta(t_1)\Delta(t_2)\cdots\Delta(t_n)\rangle_c, \tag{21}$$

where the subscript c denotes a cumulant average.[52] The cumulant average of time-ordered operators is equal to the cumulant average where each expectation value is time-ordered, as demonstrated in appendix C. So for the third order we have, using the short-hand notation $\Delta(t_i) \equiv \Delta_i$:

$$\langle T_+\Delta_1\Delta_2\Delta_3\rangle_c = \langle T_+\Delta_1\Delta_2\Delta_3\rangle - \langle\Delta_1\rangle\langle T_+\Delta_2\Delta_3\rangle - \langle\Delta_2\rangle\langle T_+\Delta_1\Delta_3\rangle - \langle\Delta_3\rangle\langle T_+\Delta_1\Delta_2\rangle + 2\langle\Delta_1\rangle\langle\Delta_2\rangle\langle\Delta_3\rangle. \tag{22}$$

Once the cumulant average has been split into products of time-ordered expectation values, we can perform the time-ordering for each expectation value. All terms involving the first

order expectation value, $\langle\Delta(t)\rangle$, vanish, since the expectation value is 0 by definition. To evaluate integrals of second- and higher-order expectation values, we use a theorem for the computation of integrals involving the matrix exponential.[53,54] Owing to the unique properties of exponential matrices, the otherwise cumbersome task of solving multiple integrals numerically is reduced to taking the exponential of a matrix. We now demonstrate this for the third order cumulant:

$$\begin{aligned}
K_3(t) =& \frac{i}{\hbar^3}\frac{1}{6}\int_0^t\int_0^t\int_0^t dt_1dt_2dt_3\langle T_+\boldsymbol{\Delta}_1\boldsymbol{\Delta}_2\boldsymbol{\Delta}_3\rangle \\
=& \frac{i}{\hbar^3}\int_0^t\int_0^{t_1}\int_0^{t_2} dt_1dt_2dt_3\langle\boldsymbol{\Delta}_1\boldsymbol{\Delta}_2\boldsymbol{\Delta}_3\rangle \\
\equiv& \frac{i}{\hbar^3}\,\mathrm{Tr}\left\{\int_0^t\int_0^{t_1}\int_0^{t_2} dt_1dt_2dt_3 e^{i\mathbf{H_g}t_1}\boldsymbol{\Delta}e^{i\mathbf{H_g}(t_2-t_1)}\boldsymbol{\Delta}e^{i\mathbf{H_g}(t_3-t_2)}\boldsymbol{\Delta}e^{-i\mathbf{H_g}t_3}\boldsymbol{\rho}_{\boldsymbol{g}}^{\boldsymbol{eq}}\right\} \\
=& \frac{i}{\hbar^3}\,\mathrm{Tr}\left\{e^{i\mathbf{H_g}t}\int_0^t\int_0^{t_1}\int_0^{t_2} dt_1dt_2dt_3 e^{-i\mathbf{H_g}(t-t_1)}\boldsymbol{\Delta}e^{-i\mathbf{H_g}(t_1-t_2)}\boldsymbol{\Delta}e^{-i\mathbf{H_g}(t_2-t_3)}\boldsymbol{\Delta}e^{-i\mathbf{H_g}t_3}\boldsymbol{\rho}_{\boldsymbol{g}}^{\boldsymbol{eq}}\right\}.
\end{aligned} \tag{23}$$

The equilibrium density matrix can be taken outside the triple integral since it is independent of the integration variables. The triple integral then has the form required by the matrix theorem, and is readily solved by first defining the auxiliary matrix

$$\mathbf{A} = \begin{pmatrix} -i\mathbf{H_g} & \boldsymbol{\Delta} & \mathbf{0} & \mathbf{0} \\ \mathbf{0} & -i\mathbf{H_g} & \boldsymbol{\Delta} & \mathbf{0} \\ \mathbf{0} & \mathbf{0} & -i\mathbf{H_g} & \boldsymbol{\Delta} \\ \mathbf{0} & \mathbf{0} & \mathbf{0} & -i\mathbf{H_g} \end{pmatrix}, \tag{24}$$

and then solving the matrix differential equation

$$\frac{d}{dt}[e^{\mathbf{A}t}] = \mathbf{A}e^{\mathbf{A}t}, \tag{25}$$

$$e^{\mathbf{A}t}\Big|_{t=0} = \mathbb{1}, \tag{26}$$

to find $e^{\mathbf{A}t}$:

$$e^{\mathbf{A}t} = \begin{pmatrix} e^{-i\mathbf{H_g}t} & \int_0^t dt_1 e^{-i\mathbf{H_g}(t-t_1)}\mathbf{\Delta}e^{-i\mathbf{H_g}t_1} & \int_0^t dt_1 \int_0^{t_1} dt_2 e^{-i\mathbf{H_g}(t-t_1)}\mathbf{\Delta}e^{-i\mathbf{H_g}(t_1-t_2)}\mathbf{\Delta}e^{-i\mathbf{H_g}t_2} & \int_0^t dt_1 \int_0^{t_1} dt_2 \int_0^{t_2} dt_3 e^{-i\mathbf{H_g}(t-t_1)}\mathbf{\Delta}e^{-i\mathbf{H_g}(t_1-t_2)}\mathbf{\Delta}e^{-i\mathbf{H_g}(t_2-t_3)}\mathbf{\Delta}e^{-i} \\ \mathbf{0} & e^{-i\mathbf{H_g}t} & \int_0^t dt_1 e^{-i\mathbf{H_g}(t-t_1)}\mathbf{\Delta}e^{-i\mathbf{H_g}t_1} & \int_0^t dt_1 \int_0^{t_1} dt_2 e^{-i\mathbf{H_g}(t-t_1)}\mathbf{\Delta}e^{-i\mathbf{H_g}(t_1-t_2)}\mathbf{\Delta}e^{-i\mathbf{H_g}t_2} \\ \mathbf{0} & \mathbf{0} & e^{-i\mathbf{H_g}t} & \int_0^t dt_1 e^{-i\mathbf{H_g}(t-t_1)}\mathbf{\Delta}e^{-i\mathbf{H_g}t_1} \\ \mathbf{0} & \mathbf{0} & \mathbf{0} & e^{-i\mathbf{H_g}t} \end{pmatrix} \tag{27}$$

The third order cumulant is then found simply as

$$K_3(t) = \frac{i}{\hbar^3}\,\mathrm{Tr}\{e^{i\mathbf{H_g}t}e_{14}^{\mathbf{A}t}\boldsymbol{\rho}_{\boldsymbol{g}}^{\boldsymbol{eq}}\}, \tag{28}$$

where $e_{14}^{\mathbf{A}t}$ is the top-right block of $e^{\mathbf{A}t}$.

Similarly, the second order cumulant is found as $K_2(t) = \frac{1}{\hbar^2}\,\mathrm{Tr}\{e^{i\mathbf{H_g}t}e_{24}^{\mathbf{A}t}\boldsymbol{\rho}_{\boldsymbol{g}}^{\boldsymbol{eq}}\}$. Incredibly, this method of solving integrals involving matrix exponentials is analytical up until the actual evaluation of $e^{\mathbf{A}t}$ which contains some approximation. We use the `expm` function implemented in Matlab to perform this task.[55,56] For a comprehensive review of the performance and limitations of a range of methods used to compute the matrix exponential, see ref 57.

For integrals of higher order expectation values, $\mathbf{A}$ must be extended in the top left corner with $-i\mathbf{H_g}$ on the diagonal and $\mathbf{\Delta}$ on the upper diagonal. Fortunately, the lower-right 4×4 block matrix of $e^{\mathbf{A}t}$ remains the same. Hence, expectation values to all orders can be calculated from a single exponential matrix, which need only be evaluated once for each t.

For $\mathbf{A}$ of order N, we can write a recursion relation for the cumulants using the short-

hand notation $B_n = (-i/\hbar)^n \,\mathrm{Tr}\{e^{i\mathbf{H_g}t} e^{\mathbf{A}t}_{N-n,N} \boldsymbol{\rho}_{\boldsymbol{g}}^{\boldsymbol{eq}}\}$. From appendix D, we have the final result as

$$K_n(t) = B_n - \sum_{m=2}^{n-2} \frac{m}{n} K_m B_{n-m}, \qquad n-2 \geq m. \tag{29}$$

The absorption lineshape function truncated at, say, sixth order in the cumulant expansion can then be calculated from a 7×7 $\mathbf{A}$ matrix as follows:

$$\mathcal{D}_{abs}(\omega - \omega_{eg}) = \frac{1}{2\pi\hbar} \,\mathrm{Re} \int_0^\infty dt e^{i(\omega-\omega_{eg})t} e^{-\gamma t} \tag{30}$$
$$\times \exp\Big[B_2 + B_3 + B_4 - B_2^2/2 + B_5 - B_2 B_3 + B_6 - B_2 B_4 - B_3^2/2 + B_2^3/3\Big].$$

The fluorescence lineshape function truncated at the same order is given as:

$$\mathcal{D}_{flu}(\omega - \omega_{eg}) = \frac{1}{2\pi\hbar} \,\mathrm{Re} \int_0^\infty dt e^{-i(\omega-\omega_{eg})t} e^{-\gamma t} \tag{31}$$
$$\times \exp\Big[\tilde{B}_2 + \tilde{B}_3 + \tilde{B}_4 - \tilde{B}_2^2/2 + \tilde{B}_5 - \tilde{B}_2 \tilde{B}_3 + \tilde{B}_6 - \tilde{B}_2 \tilde{B}_4 - \tilde{B}_3^2/2 + \tilde{B}_2^3/3\Big].$$

Here, $\tilde{B}_n = (-i/\hbar)^n \,\mathrm{Tr}\{e^{i\mathbf{H_e}t} e^{\tilde{\mathbf{A}}t}_{7-n,7} \boldsymbol{\rho}_{\boldsymbol{e}}^{\boldsymbol{eq}}\}$, where the appropriate auxiliary matrix $\tilde{\mathbf{A}}$ is found by replacing $\boldsymbol{\Delta}$ with $\tilde{\boldsymbol{\Delta}}$ and $\mathbf{H_g}$ with $\mathbf{H_e}$ in $\mathbf{A}$.

Results and Discussion

To test the two methods, we compute the absorption and fluorescence spectra of shifted Morse oscillators. The expression for the Morse potential is converted to a polynomial by Taylor expanding the exponential function to Nth order, making the Morse potential a polynomial of order $2N$. However, only the first N orders are kept to solve eq 38, since the

contributions from the higher orders are vanishingly small. N is therefore also the number of basis states. For method 1, the overlaps were calculated by numerical integration, using eigenfunctions found as linear combinations of the harmonic oscillator wavefunctions. As a benchmark, we also calculate the same spectra using analytical[58] energies and wavefunctions as input into eqs 9 and 10. Although there are ways to find analytical expressions also for the overlaps (order by order in the coordinate,[59] with the aid of recursion relationships,[60] or under an external field)[61] we chose to calculate them by numerical integration.

Fig 1 shows the results for identical Morse oscillators in the ground and excited state, with depth $D = 60\hbar\omega_0$ and width $\alpha \simeq 0.0913\sqrt{\frac{\hbar}{m\omega_0}}$, but with the excited state shifted $d = 1.6\sqrt{\frac{\hbar}{m\omega_0}}$ to the right, which resembles bond loosening upon excitation. For reference, Morse parameters for the homonuclear diatomic molecules B_2, O_2 and F_2 are approximately $\omega_0 = 1045, 1583, 894$ cm^{-1}, $D = 104.2, 201.2, 63.5$ millihartree and $\alpha = 1.89, 2.60, 2.75$ Å^{-1}, respectively, which compares well with the chosen values.[I] The temperature was set to $k_BT = 0.3\hbar\omega_0$, which is slightly less than the zero-point energy of this particular Morse oscillator: $0.499\hbar\omega_0$. 10 vibrational states were included in each electronic level, and the dephasing was set to $\gamma = 0.18\omega_0$. 40 basis states were used for method 1 and 20 basis states were used for method 2.

The absorption and fluorescence spectra are clearly not mirror images of each other. The breaking of symmetry is caused by asymmetric PESs. This anharmonic feature can not be found using the conventional methods involving shifted harmonic oscillators.

While method 1 is indistinguishable from the analytical calculation (which has been omitted in the figure), the chosen parameters prove to be a stern test for the cumulant expansion method. It was necessary to include up to 5th or 6th order in the cumulant expansion for best overall agreement with the analytical result. However, higher orders lead to divergences. In fact, already at 6th order the response function is on the brink of divergence, as is evident from the erratic behaviour at the high frequencies.

[I] Obtained by fitting the Morse potential to the ab initio ground state potential energy curves in refs 35, 36 and 62

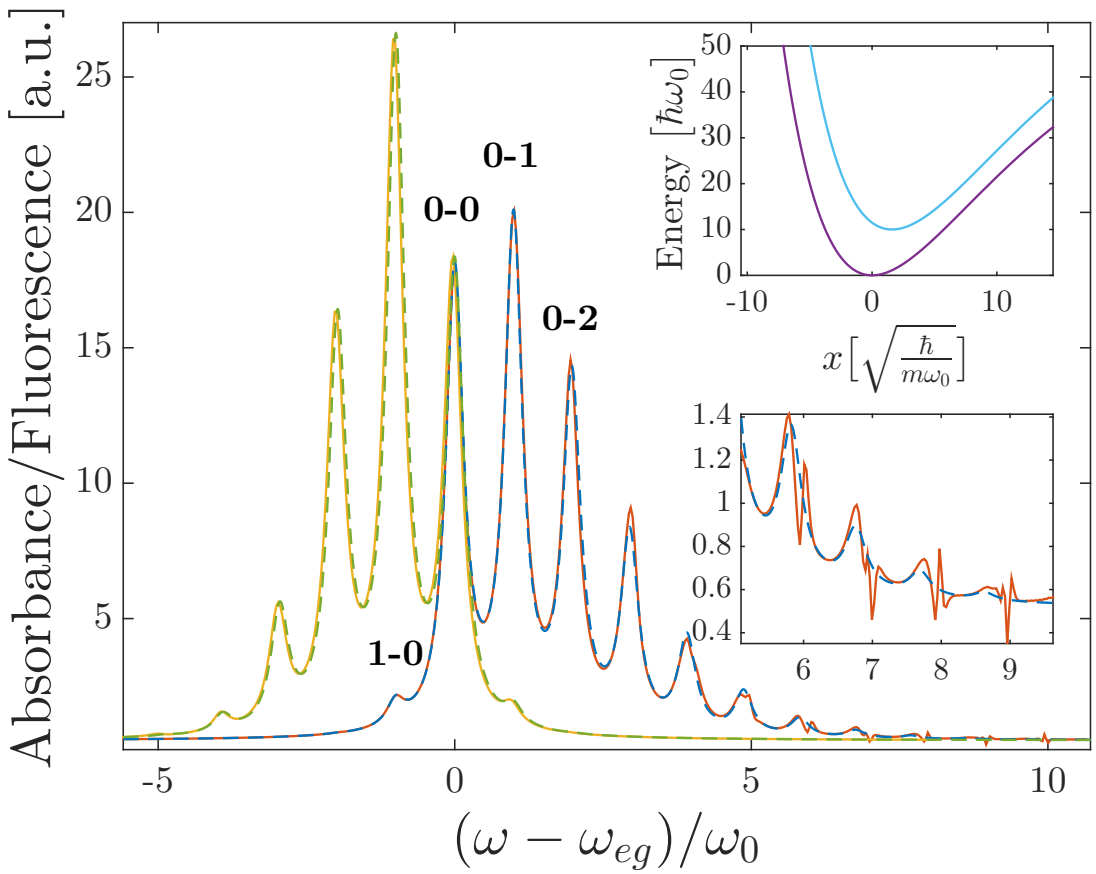

Figure 1: Absorption (dashed blue, full red) and fluorescence (dashed green, full yellow) spectra of shifted Morse oscillators. The shift is $d = 1.6\sqrt{\frac{\hbar}{m\omega_0}}$, the temperature is set to $k_BT = 0.3\hbar\omega_0$, and the dephasing is set to $\gamma = 0.18\omega_0$. Method 1 (dashed lines) produces spectra that are indistinguishable from the spectra obtained using analytical results. The cumulant expansion in method 2 (full lines) is terminated at sixth order which produces spectra that are highly accurate around $\omega \sim \omega_{eg}$, but less so in the peripheral regions of the spectra, as highlighted in the lower inset. Method 1 used 40 basis state, while method 2 used 20. The upper inset shows the PESs of the two-level system for reference. Note that the vertical offset, $\hbar\omega_{eg}$, is arbitrary. Some select absorption peaks are assigned to their vibrational transitions.

The convergence radius of the cumulant expansion is related to the instantaneous electronic energy gap, $H_e - H_g$, and the temperature. If the gap fluctuates far from the equilibrium value, low order terms will blow up sooner, and a high temperature will allow the system to explore more of the anharmonic areas (assuming the potential minima are more harmonic than the peripheral regions of the surfaces). Similar conclusions have been drawn for the

related problem of finding thermal factors for Morse oscillators and asymmetric double-wells in Extended X-Ray Absorption Fine Structure and X-ray Photoelectron Diffraction.[63,64]

While method 2 is close to reaching its limits, method 1 proves to be far more flexible. To investigate the range of applicability of method 1, we test it in more extreme cases. First, we increase the displacement to $d = 8\sqrt{\frac{\hbar}{m\omega_0}}$ and the temperature to $k_B T = 1.3\hbar\omega_0$. Higher temperatures do not present any difficulties, but have been avoided to keep the spectra simple. Absorption spectra for this system are found in Fig 2. 75 basis states were used, and the dephasing strength was kept at $\gamma = 0.18\omega_0$. The dark red spectrum is the benchmark calculated with analytical energies and wavefunctions, while the dashed blue spectrum was calculated with the methods in appendices A and B. Note that this time the overlaps were computed as inner products of the ground and excited state eigenvectors. Moreover, the excited state eigenvectors were calculated for an undisplaced excited state first, and subsequently shifted using the displacement operator, $\exp(da^\dagger - d^* a)$. This provides faster convergence than calculating the eigenvectors directly in the displaced excited state, but one should be aware that error can be introduced by the displacement operator, since the Fock space is truncated. For the direct method, we were able to converge the spectra for d between -5 and $3\sqrt{\frac{\hbar}{m\omega_0}}$ using 50 basis states, where the asymmetric interval originates from the asymmetric perturbation.

Now we put method 1 to a second test; we maintain $d = 1.6\sqrt{\frac{\hbar}{m\omega_0}}$ but vary D, the depth of the well. The width, α, is locked at $\sqrt{1/2D}$ to ensure that the harmonic term is always $x^2/2$. As D is lowered, the number of bound states decreases. Although the continuum states also have analytical expressions,[61] we disregard them in our calculations. Therefore we must also discard the states obtained numerically which correspond to higher quantum numbers than the lowest bound state, given by $[\sqrt{2mD}/\alpha\hbar - 1/2]$,[58] where $[\cdots]$ denotes rounding down to the nearest lower integer.

While the method works well for very small D, the spectra are less interesting when the number of bound states is one or two. Instead we show in Fig 3 the results for $D = 3\hbar\omega_0$

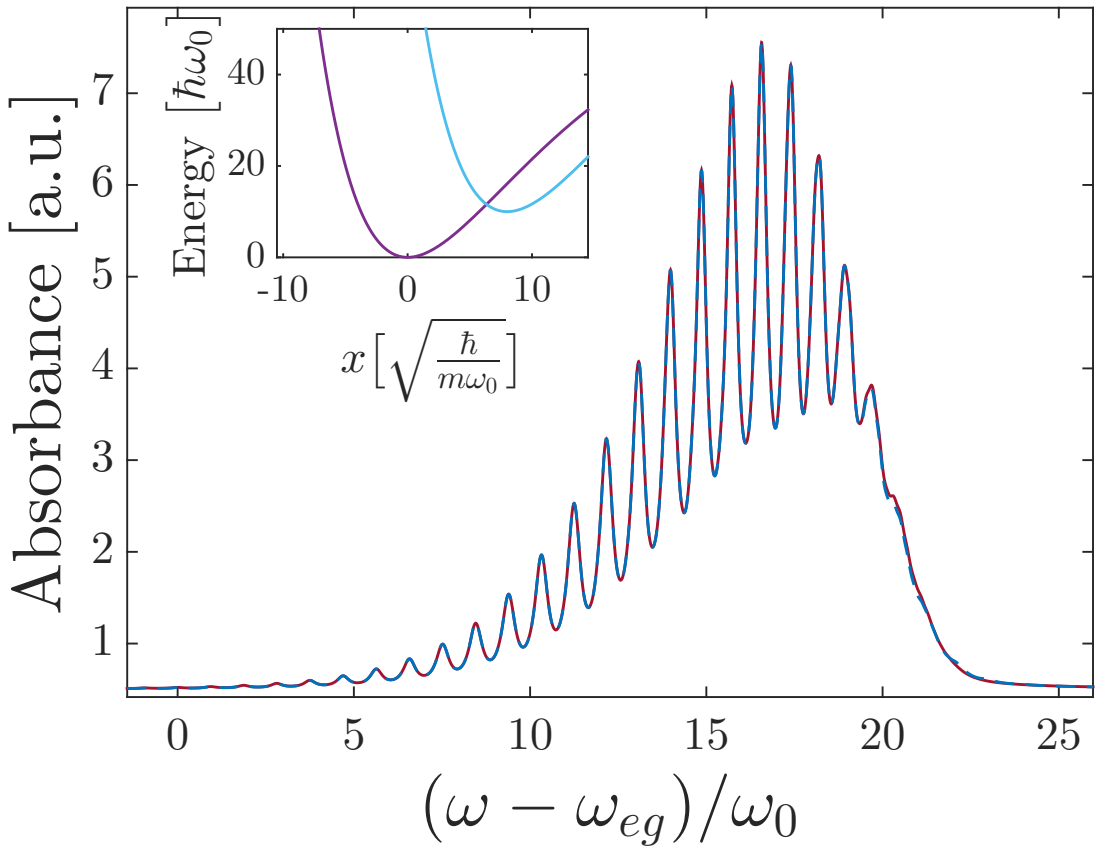

Figure 2: Absorption spectra of shifted Morse oscillators. The shift is $d = 8\sqrt{\frac{\hbar}{m\omega_0}}$, the temperature is $k_BT = 1.3\hbar\omega_0$, and the dephasing is $0.18\omega_0$. The dark red line is the analytical result, while the dashed blue line was calculated numerically using the methods described in appendices A and B, with the intermediate step of first finding the excited state wavefunctions for an undisplaced potential, and translate them afterwards using the displacement operator. 75 basis states were used to calculate the vibrational energies and eigenstates, and 35 vibrational states in each electronic level were used to calculate both spectra. The upper inset shows the PESs of the two-level system for reference.

which has six bound states. 170 basis states were used, but this time only 70 orders in the perturbation, i.e. $M = 70$ in eq 34, for practical reasons. The temperature was set to $k_B T = 1.3\hbar\omega_0$ and the dephasing strength set to $\gamma = 0.06\omega_0$. The overlaps were again calculated as inner products with the intermediate step of the displacement operator. Note, though, that if instead the displacement were $d = -1.6\sqrt{\frac{\hbar}{m\omega_0}}$, faster convergence would be obtained with the direct method (without the displacement operator), since in that case the perturbation from H_0 would be smaller in the displaced excited state.

The ZPLs in the absorption spectra are symmetric since the vibrational energy levels are the same for the ground and excited state. However, when the absorption involves emission of a phonon, there is strong splitting of the peak that is constituted by the 1-0, 2-1, 3-2 transitions etc., since these energy spacings are different.

Having thoroughly tested method 1 and method 2 for various systems of shifted Morse oscillators, we apply method 1 to a generic two-level system, to demonstrate the possibilities that open up when the surfaces are not restricted to the harmonic oscillator or the Morse oscillator. We define a system where the vibrational energy spacings are different for the ground and excited state, with $V_g(x) = 0.2x^4 - 0.75x^3 + 0.875x^2$ and $V_e(x) = 0.2(x-1)^4$. While there are no exact solutions for quartic potentials, we are confident that the energies and wavefunctions are highly accurate, since the perturbation from H_0 is smaller than for the cases we have already considered. Moreover, the first 10 energy levels of the pure quartic oscillator matched those in ref 65 to the fourth decimal.

This system can give rise to a splitting of the ZPL, as this peak is consituted by purely electronic transitions; 0-0, 1-1, 2-2 etc., which will have different energies since the PESs are different. To see the splitting, it is necessary for the vibrational states to be excited prior to the excitation pulse, in order to see anything but the 0-0 transition. This requires a high temperature, which is why the use of method 2 was prohibited. Ideally, a comparison to method 2 would help bolster the results in the absence of an analytical benchmark, since it would be unlikely that the two methods produce the same spectra, given how different they

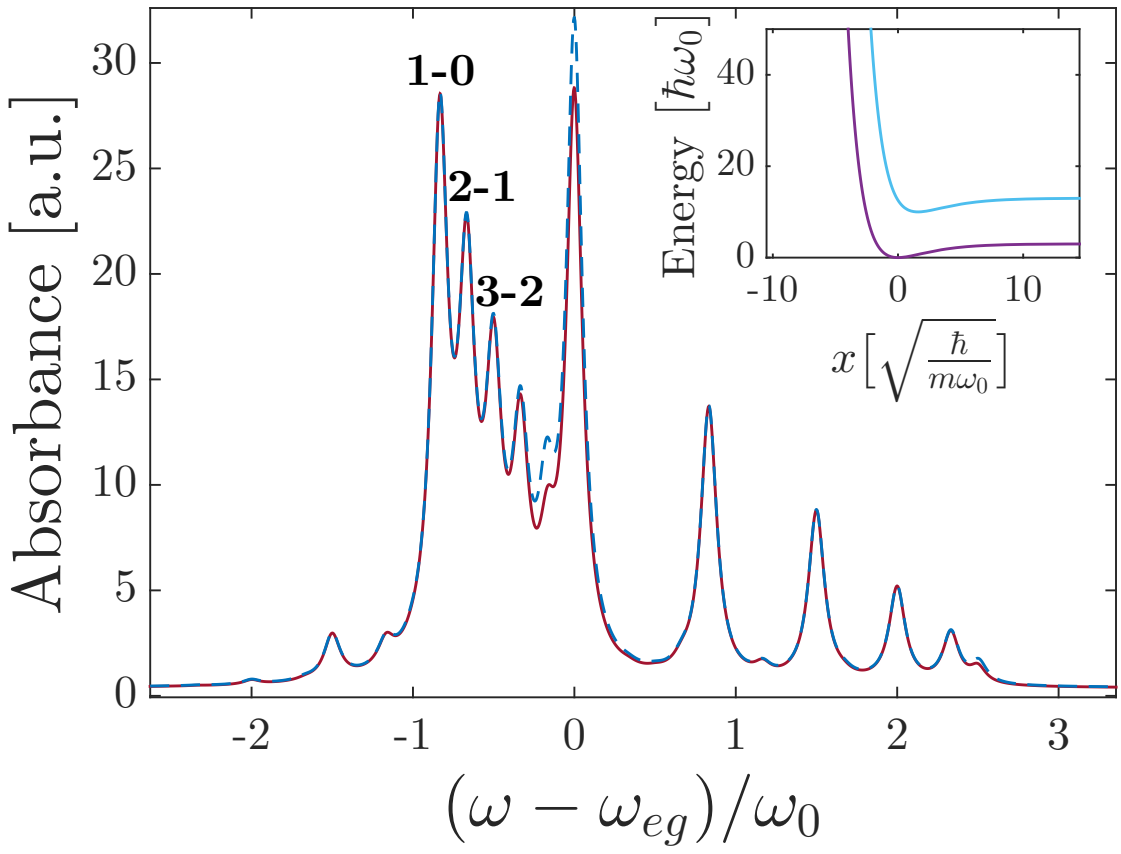

Figure 3: Absorption spectra of shifted Morse oscillators. The shift is $d = 1.6\sqrt{\frac{\hbar}{m\omega_0}}$ and temperature is set to $k_BT = 1.3\hbar\omega_0$. The dark red line is the analytical result, while the blue was calculated numerically by finding the excited state wavefunctions for an undisplaced potential, and subsequently move them using the displacement operator, before calculating the overlaps as inner products. Note that the excited state energies also were calculated in the undisplaced potential, since they converged more quickly towards the analytical solutions there.

are. Unfortunately, the cumulant expansion is ill-behaved at high temperatures when the ground and excited state surfaces are sufficiently different.

We perform the calculations with 40 basis states at $k_BT = 6.3\hbar\omega_0$ and $\gamma = 0.03\omega_0$. The absorption spectrum is shown in Fig 4. The jagged structure of the ZPL is the third anharmonic feature encountered in this work. This feature can also be obtained using harmonic oscillators with differing curvatures, but one still needs to use a method that accounts for the nonlinear electronic-vibrational coupling.

The drawback of method 1 is that the energies and eigenfunctions are not exact, unless the potentials belong to a very restricted class of functions that have analytical solutions. The cumulant expansion method, on the other hand, is in principle exact, but suffers when the anharmonicity is large and when the temperature is high. Method 2 is also harder to work with as one has to make a choice of how many terms to include in the cumulant expansion, which can make it difficult to know when convergence is reached, although it is quite evident when it fails. In light of our findings, we deem method 1 to be superior to method 2. The biggest concern is whether the numerically determined energies and the wavefunctions are close to their true counterparts. Our experience is that even in quite extreme cases, a high fidelity is achieved, and it becomes mostly a matter of including sufficiently many basis states. Combined with the fact that it is often only the first several vibrational states that are relevant in spectroscopy, the method is safe to use.

The shifted Morse oscillator system was chosen because it is one of the very few potentials that can be solved analytically, which enabled benchmarking. However, a polynomial is not the ideal function for describing decaying potentials, since the polynomial inevitably diverges. So although the methods developed in this work perform well for the decaying Morse potential, the natural domain for these methods will be confining potentials, where steep rises in the potential energy at both edges are effortlessly handled by a relatively low-order polynomial. The methods will also be adept at handling highly curved potentials. A system that could be particularly interesting to explore with these methods is that of the

oscillating proton in a hydrogen bond, which can have diverse potentials, depending on the nature of the bond, many of which will be inadequately described by the harmonic or Morse potential.

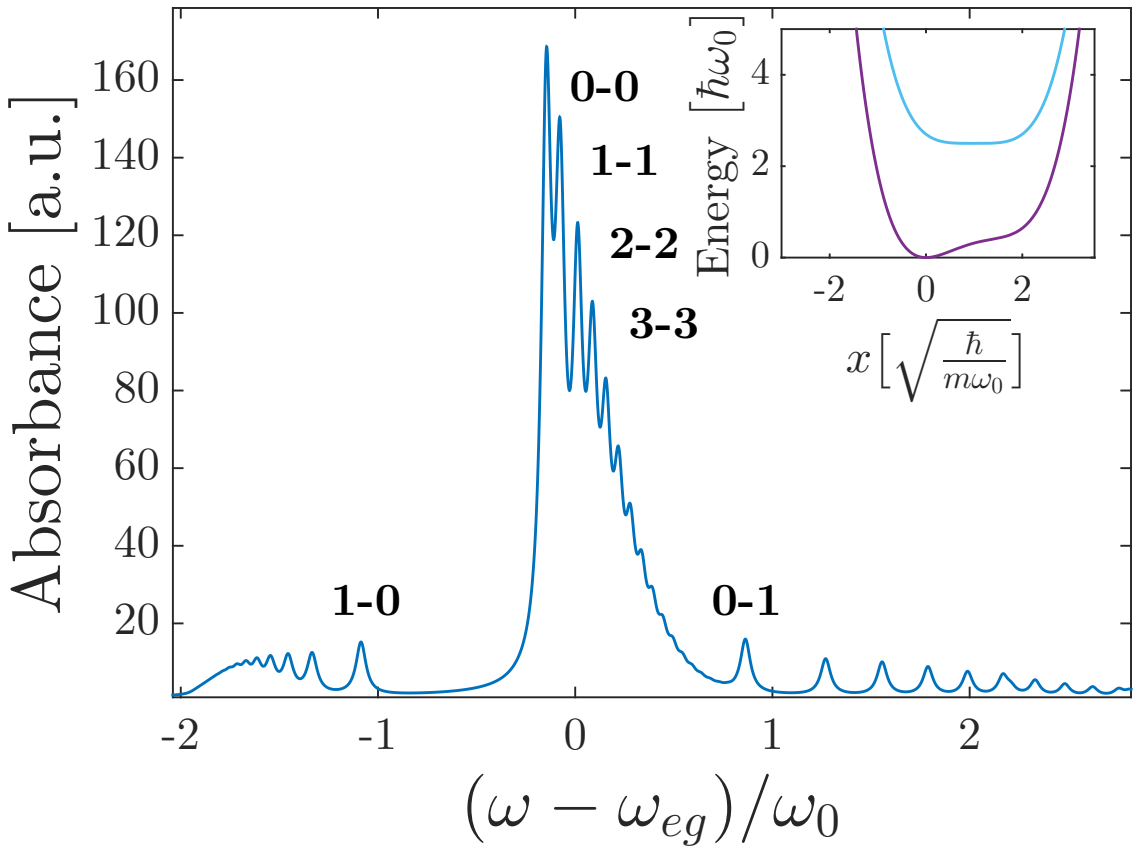

Figure 4: Absorption spectra calculated with method 1 using 40 basis states, at a temperature of $k_BT = 6.3\hbar\omega_0$ with a dephasing strength of $\gamma = 0.03\omega_0$. The purely electronic transitions that together make up the ZPL no longer coincide since the transitions frequencies are different. This gives a structure to the ZPL which can only be seen using anharmonic methods. The upper inset shows the potentials which are given by $V_g(x) = 0.2x^4 - 0.75x^3 + 0.875x^2$ and $V_e(x) = 0.2(x-1)^4$.

Numerical Considerations

The speed of the calculations is largely a question of how many states are needed to represent the wavefunctions or the electronic gap, and additionally for method 1 how many orders are needed to represent the perturbation potential. On a local computer, the time it takes to

compute a spectrum can range from a couple of seconds to a few minutes. Most realistic systems, however, are not as anharmonic as those we have considered here.

For method 2, we compared (trapezoidal) numerical integration and matrix exponential integration for a system with 22 basis states. The numerical integrations of a triple and a quadruple integral with 100 and 10 time steps for each time variable, respectively, clocked in at two and a half minutes and six and a half minutes. The same calculations took less than a second with the matrix exponential method. Besides the improvement of speed, the matrix exponential method also scales much better, making it feasible to calculate high-order cumulants.

Summary

In this paper, we have discussed two different methods to calculate linear absorption and fluorescence spectra for an electronic two-level system with polynomial PESs. The first method takes a polynomial perturbation potential with respect to the harmonic oscillator, and diagonalises the Hamiltonian to find energies and wavefunctions as linear combinations of the harmonic oscillator wavefunctions. The optical response functions are then found by summing all Liouville pathways. The second method employs the cumulant expansion to calculate the spectra. Using an ideally suited matrix theorem, we show that the evaluation of the integrals is highly efficient.

While the first method can tackle virtually any realistic, anharmonic system, the second method encounters divergence problems at large anharmonicities and temperatures. Although we recommend the first method for the calculation of optical spectra, we believe the second method to be of equal interest due to the way the integrals of the response functions are handled. This could potentially bring great speedups for similar calculations, even outside of spectroscopy.

Using these methods, we were able to study anharmonic features like mirror-symmetry

breaking between absorption and fluorescence, and splitting of the ZPL and the one-phonon peak. The developed methods pave way for using quantum chemical potential energy surfaces as input to obtain more detailed spectra of systems involving anharmonic oscillators. A natural next step for the methods would be to simulate experimental spectra of vibrational modes that are poorly described by the standard harmonic or Morse potentials. An extension to higher dimensions would also be interesting as that would facilitate the study of concerted motion on multivariate polynomial surfaces, such as processes involving conical intersections.[66,67]

Acknowledgements

TH is grateful for financial support from the Lundbeck Foundation. DA acknowledges the support by Research Council of Lithuania, projects MIP-090/2015.

A Calculation of Energy Eigenvalues

This section summarises the method in ref 46 used to calculate the energy eigenvalues, which will also enable the calculation of the vibrational wavefunctions. The starting point is to find generalised creation and annihilation operators by performing a Bogoliubov transformation of the ordinary creation and annihilation operators of the harmonic oscillator, $a^\dagger = \frac{x+ip}{\sqrt{2}}$ and $a = \frac{x-ip}{\sqrt{2}}$:

$$b^\dagger = \frac{a^\dagger - ta}{\sqrt{1-t^2}}, \qquad b = \frac{a - ta^\dagger}{\sqrt{1-t^2}}, \tag{32}$$

where t is a real number satisfying $|t|^2 < 1$. Both sets of operators obey the commutation relation $[a, a^\dagger] = [b, b^\dagger] = 1$. The next step is to use a squeezed vacuum state, $|0, t\rangle = (1-t^2)^{\frac{1}{4}} \exp(\frac{t}{2} a^{\dagger 2})|0\rangle$, as a one-parameter trial wavefunction. (Here $|0\rangle$ is the harmonic oscillator vacuum state.) Energy minimisation with respect to the squeezing parameter

will find the vacuum state of the generalised number states. The remaining generalised number states can then be generated by repeated application of the new creation operator: $|n,t\rangle = \frac{b^{\dagger n}}{\sqrt{n!}}|0,t\rangle$. Consistently, b is the annihilation operator: $b|0,t\rangle = 0$. The infinite set of $|n,t\rangle$ is complete and orthonormal. A truncated set is later used to find the eigenvalues.

The energy minimisation requires $H_{anh} = \frac{1}{2} + a^\dagger a + \sum_m \lambda_m (\frac{a+a^\dagger}{\sqrt{2}})^m$ to be expressed by $b^\dagger$ and b. For this purpose, it is convenient to normal-order the ladder operators:

$$(b+b^\dagger)^m = \sum_{k=0}^{[m/2]} \frac{m!}{2^k k!} \sum_{j=0}^{m-2k} \frac{b^{\dagger m-2k-j} b^j}{j!(m-2k-j)!}, \tag{33}$$

where $[\cdots]$ denotes rounding down to the nearest integer. By redefining the squeezing parameter as $\Omega = \frac{1-t}{1+t}$ the final expression becomes more compact:

$$H_{anh} = \frac{1}{2} + \frac{(1-\Omega)^2}{4\Omega} + \frac{1+\Omega^2}{2\Omega} b^\dagger b + \frac{1-\Omega^2}{4\Omega}(b^2 + b^{\dagger 2}) + \sum_{m=0}^{M} \frac{\lambda_m}{(2\Omega)^{m/2}} \sum_{k=0}^{[m/2]} \sum_{n=0}^{m-2k} \frac{m! b^{\dagger m-2k-n} b^n}{2^k k! n! (m-2k-n)!}. \tag{34}$$

Now we can calculate the expectation value of the energy as

$$\varepsilon(\Omega) = \langle 0,\Omega|H|0,\Omega\rangle = \frac{1}{2} + \frac{(1-\Omega)^2}{4\Omega} + \sum_{m=0,2,4,\ldots}^{\{M\}} \frac{\lambda_m m!}{2^m \Omega^{(m/2)} (m/2)!}, \tag{35}$$

where $\{M\}$ denotes the largest even number which is equal to or less than M, the degree of the polynomial. By minimising the expectation value, we find the equation for the optimal value of Ω_0:

$$1 - \frac{1}{\Omega_0^2} + \sum_{m=2,4,\ldots}^{\{M\}} \frac{\lambda_m m!}{2^{m-2} \Omega_0^{(m/2+1)} [(m/2-1)]!} = 0. \tag{36}$$

This eq can be solved numerically. Once Ω_0 is determined for the squeezed vacuum state, the optimal generalised number states are generated using

$$|n, \Omega_0\rangle = \frac{b^{\dagger n}}{\sqrt{n!}}|0, \Omega_0\rangle. \tag{37}$$

These will be the basis functions used to construct the Hamiltonian matrix below. Since the basis functions are not eigenfunctions of H_{anh} the matrix will in general not be diagonal.

$$H_{anh,ij} = \left[\frac{1+\Omega_0^2}{4\Omega_0} + \frac{1+\Omega_0^2}{2\Omega_0} j\right]\delta_{ij} + \frac{1-\Omega_0^2}{4\Omega_0}\Big\{[j(j-1)]^{\frac{1}{2}}\delta_{i,j-2} + [(j+1)(j+2)]^{\frac{1}{2}}\delta_{i,j+2}\Big\} + \sum_{m=0}^{M}\sum_{k=0}^{[m/2]}\sum_{n=0}^{m-2k} \frac{\lambda_m m![j!(j+m-2k-2n)!]^{\frac{1}{2}}}{(2\Omega_0)^{(m/2)}2^k k!n!(j-n)!(m-2k-n)!}\delta_{1,j+m-2k-2n}. \tag{38}$$

After truncation and diagonalisation, we have the eigenvalues of the quantum anharmonic oscillator. However, truncation lifts orthogonality and normalisation for the states that are close to the truncation boundary. Extra care should therefore be taken to ensure a well-behaved system.

B Calculation of Vibrational Wavefunctions

To calculate the vibrational wavefunctions, one can exploit the fact that the eigenfunctions of the harmonic oscillator are known. By mapping the eigenstates of the anharmonic oscillator to the harmonic oscillator basis, they can be expressed as linear combinations of the harmonic oscillator wavefunctions. For a general eigenstate $|\chi_\alpha\rangle$ taken as an eigenvector from the above diagonalisation, we then have

$$|\chi_\alpha\rangle = \begin{pmatrix} \alpha_0 \\ \alpha_1 \\ \vdots \\ \alpha_N \end{pmatrix} = \sum_{n=0}^{N} \alpha_n |n, t_0\rangle = \sum_{n=0}^{N} \frac{\alpha_n b^{\dagger n}}{\sqrt{n!}} |0, t_0\rangle \tag{39}$$
$$= \sum_{n=0}^{N} \frac{\alpha_n (a^\dagger - t_0 a)^n}{\sqrt{(1-t_0^2)n!}} (1-t_0^2)^{\frac{1}{4}} \exp(\tfrac{t_0}{2} a^{\dagger 2}) |0\rangle \equiv \sum_{n=0}^{N} c_n |n\rangle.$$

The coordinate representation then gives the wavefunctions $\langle x| \sum_{n=0}^{N} c_n |n\rangle = \sum_{n=0}^{N} c_n \psi_n$, where $\psi_n = \frac{1}{\sqrt{2^n n!}} \pi^{-\frac{1}{4}} e^{-\frac{1}{2}x^2} H_n(x)$ are the well-known solutions for the harmonic oscillator and H_n is the nth order Hermite polynomial.

In method 1, the calculation of lineshape functions requires the overlaps between ground and excited state vibrational wavefunctions, $\langle \chi_{gM} | \chi_{eN} \rangle$. These inner products can be calculated in a number of ways. One approach is to compute the integrals over wavefunctions numerically. It is then advisable to calculate the excited state vibrational wavefunctions without a shift relative to the ground state vibrational wavefunctions, and only introduce the shift manually when performing the numerical integration. The downside of this method is that it is rather slow.

Alternatively, one can compute the overlaps as inner products of the eigenvectors found using 39, either directly on the defined two-level system, or by first finding the eigenvectors for an undisplaced excited state and subsequently shift them using the displacement operator, $\exp(da^\dagger - d^* a)$, where d is the distance. The choice depends on which excited state, the displaced or undisplaced, has the smallest perturbation with respect to the harmonic oscillator, since a smaller perturbation improves accuracy. This will normally be the undisplaced excited state (but not always). However, one must be careful with the displacement operator since it can distort the states upon shifting them. This is due to the truncation of the Fock space and is mostly relevant for the higher excited vibrational states. The error

can always be made smaller by expanding the basis set. This method is much faster than numerical integration, and should be preferred for most applications.

C Time-Ordered Cumulant Expansion

To see how time-ordering affects the cumulant expansion, we calculate the first few cumulants in the following. The starting point is to postulate that

$$\left\langle T_+ \exp\left\{ \int_0^t dt_1 X(t_1) \right\} \right\rangle = \exp\left\{ \sum_{n=1}^{\infty} \int_0^t dt_1 \cdots \int_0^t dt_n \frac{1}{n!} \langle T_+ X(t_1) \cdots X(t_n) \rangle_c \right\}, \tag{40}$$

and then to expand both sides of the equation and comparing terms at each order. In the main text, $X(t)$ is replaced by $-\frac{i}{\hbar}\Delta(t)$. The LHS becomes

$$\begin{aligned} & 1 + \int_0^t dt_1 \langle X(t_1) \rangle + \frac{1}{2!} \int_0^t \int_0^t dt_1 dt_2 \langle T_+ X(t_1) X(t_2) \rangle \\ & + \frac{1}{3!} \int_0^t \int_0^t \int_0^t dt_1 dt_2 dt_3 \langle T_+ X(t_1) X(t_2) X(t_3) \rangle \\ & + \frac{1}{4!} \int_0^t \int_0^t \int_0^t \int_0^t dt_1 dt_2 dt_3 dt_4 \langle T_+ X(t_1) X(t_2) X(t_3) X(t_4) \rangle + ..., \end{aligned} \tag{41}$$

while the RHS becomes

$$1+\sum_{n=1}^{\infty}\int_0^t dt_1\cdots\int_0^t dt_n\frac{1}{n!}\langle T_+X(t_1)\cdots X(t_n)\rangle_c \tag{42}$$
$$+\frac{1}{2!}\left[\sum_{n=1}^{\infty}\int_0^t dt_1\cdots\int_0^t dt_n\frac{1}{n!}\langle T_+X(t_1)\cdots X(t_n)\rangle_c\right]^2$$
$$+\frac{1}{3!}\left[\sum_{n=1}^{\infty}\int_0^t dt_1\cdots\int_0^t dt_n\frac{1}{n!}\langle T_+X(t_1)\cdots X(t_n)\rangle_c\right]^3$$
$$+\frac{1}{4!}\left[\sum_{n=1}^{\infty}\int_0^t dt_1\cdots\int_0^t dt_n\frac{1}{n!}\langle T_+X(t_1)\cdots X(t_n)\rangle_c\right]^4+...$$

There is only one linear term on each side of the equation, so we find

$$\int_0^t dt_1\langle X(t_1)\rangle=\int_0^t dt_1\langle X(t_1)\rangle_c$$
$$\Rightarrow\langle X(t_1)\rangle_c=\langle X(t_1)\rangle. \tag{43}$$

Comparing second order terms, we get

$$\frac{1}{2}\int_0^t\int_0^t dt_1dt_2\langle T_+X(t_1)X(t_2)\rangle=\frac{1}{2}\int_0^t\int_0^t dt_1dt_2\langle T_+X(t_1)X(t_2)\rangle_c+\frac{1}{2}\int_0^t dt_1\langle X(t_1)\rangle_c\int_0^t dt_2\langle X(t_2)\rangle_c$$
$$\Rightarrow\langle T_+X(t_1)X(t_2)\rangle_c=\langle T_+X(t_1)X(t_2)\rangle-\langle X(t_1)\rangle\langle X(t_2)\rangle. \tag{44}$$

At third order we have

$$\frac{1}{6}\int_0^t\int_0^t\int_0^t dt_1dt_2dt_3\langle T_+X(t_1)X(t_2)X(t_3)\rangle = \frac{1}{6}\int_0^t\int_0^t\int_0^t dt_1dt_2dt_3\langle T_+X(t_1)X(t_2)X(t_3)\rangle_c \tag{45}$$
$$+\frac{1}{2}\int_0^t dt_1\langle X(t_1)\rangle_c\int_0^t\int_0^t dt_2dt_3\langle T_+X(t_2)X(t_3)\rangle_c$$
$$+\frac{1}{6}\int_0^t dt_1\langle X(t_1)\rangle_c\int_0^t dt_2\langle X(t_2)\rangle_c\int_0^t dt_3\langle X(t_3)\rangle_c.$$

Inserting the first and second order cumulants, 43 and 44, we find

$$\int_0^t\int_0^t\int_0^t dt_1dt_2dt_3\langle T_+X(t_1)X(t_2)X(t_3)\rangle_c = \int_0^t\int_0^t\int_0^t dt_1dt_2dt_3\langle T_+X(t_1)X(t_2)X(t_3)\rangle$$
$$-3\int_0^t dt_1\langle X(t_1)\rangle\int_0^t\int_0^t dt_2dt_3\langle T_+X(t_2)X(t_3)\rangle$$
$$+2\int_0^t dt_1\langle X(t_1)\rangle\int_0^t dt_2\langle X(t_2)\rangle\int_0^t dt_3\langle X(t_3)\rangle$$
$$\Rightarrow \langle T_+X(t_1)X(t_2)X(t_3)\rangle_c = \langle T_+X(t_1)X(t_2)X(t_3)\rangle - 3\langle X(t_1)\rangle\langle T_+X(t_2)X(t_3)\rangle$$
$$+2\langle X(t_1)\rangle\langle X(t_2)\rangle\langle X(t_3)\rangle. \tag{46}$$

Collecting quartic terms, we get

$$
\begin{aligned}
&\frac{1}{24}\int_0^t\int_0^t\int_0^t\int_0^t dt_1dt_2dt_3dt_4\langle T_+X(t_1)X(t_2)X(t_3)X(t_4)\rangle \qquad (47)\\
&=\frac{1}{24}\int_0^t\int_0^t\int_0^t\int_0^t dt_1dt_2dt_3dt_4\langle T_+X(t_1)X(t_2)X(t_3)X(t_4)\rangle_c\\
&+\frac{1}{6}\int_0^t dt_1\langle X(t_1)\rangle_c\int_0^t\int_0^t\int_0^t dt_2dt_3dt_4\langle T_+X(t_2)X(t_3)X(t_4)\rangle_c\\
&+\frac{1}{8}\int_0^t\int_0^t dt_1dt_2\langle T_+X(t_1)X(t_2)\rangle_c\int_0^t\int_0^t dt_3dt_4\langle T_+X(t_3)X(t_4)\rangle_c\\
&+\frac{1}{4}\int_0^t dt_1\langle X(t_1)\rangle_c\int_0^t dt_2\langle X(t_2)\rangle_c\int_0^t\int_0^t dt_3dt_4\langle T_+X(t_3)X(t_4)\rangle_c\\
&+\frac{1}{24}\int_0^t dt_1\langle X(t_1)\rangle_c\int_0^t dt_2\langle X(t_2)\rangle_c\int_0^t dt_3\langle X(t_3)\rangle_c\int_0^t dt_4\langle X(t_4)\rangle_c.
\end{aligned}
$$

To solve for the fourth order cumulant, we insert the lower order cumulants and find

$$
\begin{aligned}
&\Rightarrow\langle T_+X(t_1)X(t_2)X(t_3)X(t_4)\rangle_c=\langle T_+X(t_1)X(t_2)X(t_3)X(t_4)\rangle-4\langle X(t_1)\rangle\langle T_+X(t_2)X(t_3)X(t_4)\rangle \qquad (48)\\
&-3\langle T_+X(t_1)X(t_2)\rangle\langle T_+X(t_3)X(t_4)\rangle+12\langle T_+X(t_1)X(t_2)\rangle\langle X(t_3)\rangle\langle X(t_4)\rangle\\
&-6\langle X(t_1)\rangle\langle X(t_2)\rangle\langle X(t_3)\rangle\langle X(t_4)\rangle.
\end{aligned}
$$

A pattern emerges where the time-ordered cumulant expansion is the ordinary cumulant expansion with time-ordered expectation values.

D Recursion Relation for the Cumulants

The ordinary recursion relation for computing cumulants from moments is given by[68]

$$K_n(t) = \mu_n - \sum_{m=1}^{n-1} \binom{n-1}{m-1} K_m \mu_{n-m}. \tag{49}$$

In our case, we must also include the factorials that are produced when performing the time-ordering, so we get

$$K_n(t) = B_n - \sum_{m=2}^{n-2} \binom{n-1}{m-1} K_m \frac{(n-m)!m!}{n!} B_{n-m} = B_n - \sum_{m=2}^{n-2} \frac{m}{n} K_m B_{n-m}, \qquad n-2 \geq m, \tag{50}$$

where $B_n = (-i/\hbar)^n \operatorname{Tr}\{e^{i\mathbf{H_g}t} e^{\mathbf{A}t}_{N-n,N} \boldsymbol{\rho}_{\boldsymbol{g}}^{\boldsymbol{eq}}\}$, and $\mathbf{A}$ is the $N \times N$ block matrix found by extending eq 24 with $-i\mathbf{H_g}$ along the diagonal and with $\boldsymbol{\Delta}$ along the upper diagonal towards the top-left corner. Note that $K_1(t) = B_1 = 0$ making $K_2(t)$ the first non-zero cumulant.

E Liouville Space Formulation of the Cumulants

To allow for more general dissipation mechanisms we formulate the cumulants in Liouville space, in order to maintain the same mathematical structure and hence compatibility with the matrix theorem. Standard Markovian master equations such as the Lindblad equation and various flavours of the Redfield equation can then be employed to propagate the quantum system.[48,49] Although there are many equivalent ways to map the equations from Hilbert space to Liouville space, we recommend the one in refs 69 and 70 where the density matrix is reordered into a vector by appending columns from left to right. The corresponding transformation of operators into superoperators is then

$$A\rho B \underset{Hilbert}{\overset{Liouville}{\rightleftharpoons}} (B^T \otimes A)\rho. \tag{51}$$

By solving the equation of motion for the open quantum system, the time evolution

operator is found as $e^{\boldsymbol{\mathcal{L}}t} \equiv e^{\left[\mathbb{1}\otimes(-i\mathbf{H_g})+(i\mathbf{H_g})^T\otimes\mathbb{1}-\mathcal{R}\right]t}$, where $\mathcal{R}$ is the method-specific dissipator.

By making the transformation to Liouville space and replacing the coherent time-evolution operators with dissipative ones, the cumulants can be found. For the third-order cumulant, eq 23, we then get

$$\mathcal{K}_3(t) = \frac{i}{\hbar^3}\,\mathrm{Tr}\left\{e^{\tilde{\boldsymbol{\mathcal{L}}}t}\int_0^t\int_0^{t_1}\int_0^{t_2} dt_1dt_2dt_3 e^{\boldsymbol{\mathcal{L}}(t-t_1)}\boldsymbol{\Delta}e^{\boldsymbol{\mathcal{L}}(t_1-t_2)}\boldsymbol{\Delta}e^{\boldsymbol{\mathcal{L}}(t_2-t_3)}\boldsymbol{\Delta}e^{\boldsymbol{\mathcal{L}}t_3}\boldsymbol{\rho}_{\boldsymbol{g}}^{\boldsymbol{eq}}\right\}, \tag{52}$$

where $\boldsymbol{\Delta} = \mathbb{1}\otimes\boldsymbol{\Delta}$ and $\tilde{\boldsymbol{\mathcal{L}}}$ is the reverse-time generator which can be found if the steady state with respect to $e^{\boldsymbol{\mathcal{L}}t}$ is known.[71]

At this point we can apply the matrix theorem and find the third order cumulant as

$$\mathcal{K}_3(t) = \frac{i}{\hbar^3}\,\mathrm{Tr}\{e^{\tilde{\boldsymbol{\mathcal{L}}}t}e^{\boldsymbol{\mathcal{A}}t}_{N-3,N}\boldsymbol{\rho}_{\boldsymbol{g}}^{\boldsymbol{eq}}\}, \tag{53}$$

where $\boldsymbol{\mathcal{A}}$ is found by replacing the diagonal blocks of $\mathbf{A}$ with $\boldsymbol{\mathcal{L}}$ and the off-diagonal blocks with $\boldsymbol{\Delta}$. The procedure for finding the second- and higher-order cumulants is analogous.

While the extension to Liouville space opens the possibility to study anharmonic and dissipative effects within the same framework, the price to pay is dear since the matrix size increases from $N \times N$ to $N^2 \times N^2$.

References

(1) Romero, E.; Augulis, R.; Novoderezhkin, V. I.; Ferretti, M.; Thieme, J.; Zigmantas, D.; van Grondelle, R. *Nat. Phys.* **2014**, *10*, 676–682.

(2) Fuller, F. D.; Pan, J.; Gelzinis, A.; Butkus, V.; Senlik, S. S.; Wilcox, D. E.; Yocum, C. F.; Valkunas, L.; Abramavicius, D.; Ogilvie, J. P. *Nat. Chem.* **2014**, *6*, 706–711.

(3) Pieper, J.; Freiberg, A. In *The Biophysics of Photosynthesis*; Golbeck, J., van der Est, A., Eds.; Springer New York: New York, NY, 2014; pp 45–77.

(4) Rancova, O.; Jankowiak, R.; Abramavicius, D. *J. Chem. Phys.* **2015**, *142*, 212428.

(5) Rancova, O.; Abramavicius, D. *J. Phys. Chem. B* **2014**, *118*, 7533–7540.

(6) Denisov, G. S.; Mavri, J.; Sobczyk, L. In *Hydrogen Bonding—New Insights*; Grabowski, S. J., Ed.; Springer Netherlands: Dordrecht, 2006; pp 377–416.

(7) Grabowski, S. J. *Annu. Rep. Prog. Chem., Sect. C: Phys. Chem.* **2006**, *102*, 131–165.

(8) Kwac, K.; Lee, H.; Cho, M. *J. Chem. Phys.* **2004**, *120*, 1477–1490.

(9) Garrett-Roe, S.; Hamm, P. *J. Chem. Phys.* **2008**, *128*, 104507.

(10) Olbrich, C.; Jansen, T. L. C.; Liebers, J.; Aghtar, M.; Strümpfer, J.; Schulten, K.; Knoester, J.; Kleinekathöfer, U. *J. Phys. Chem. B* **2011**, *115*, 8609–8621.

(11) Hamm, P. *J. Chem. Phys.* **2006**, *124*, 124506.

(12) Jansen, T. L. C.; Knoester, J. *J. Chem. Phys.* **2007**, *127*, 234502.

(13) Packwood, D. M.; Tanimura, Y. *Phys. Rev. E* **2011**, *84*, 61111.

(14) Osad'ko, I. S. *Zh. Eksp. Teor. Fi.* **1977**, *72*, 1575–1588.

(15) Osad'ko, I. S. *Sov. Phys. Usp.* **1979**, *22*, 311.

(16) Hizhnyakov, V. V. *Phys. Status Solidi B* **1982**, *114*, 721–730.

(17) Skinner, J. L.; Hsu, D. *J. Phys. Chem.* **1986**, *90*, 4931–4938.

(18) Hsu, D.; Skinner, J. L. *J. Lumin.* **1987**, *37*, 331–337.

(19) Hizhnyakov, V. *J. Phys. C* **1987**, *20*, 6073.

(20) Barsegov, V.; Chernyak, V.; Mukamel, S. *Isr. J. Chem.* **2002**, *42*, 143–149.

(21) Fidler, A. F.; Engel, G. S. *J. Phys. Chem. A* **2013**, *117*, 9444–9453.

(22) Tanimura, Y.; Okumura, K. *J. Chem. Phys.* **1997**, *106*, 2078–2095.

(23) Jansen, T. l. C.; Mukamel, S. *J. Chem. Phys.* **2003**, *119*.

(24) Šanda, F.; Perlík, V.; Lincoln, C. N.; Hauer, J. *J. Phys. Chem. A* **2015**, *119*, 10893–10909.

(25) Roy, S.; Pshenichnikov, M. S.; Jansen, T. L. C. *J. Phys. Chem. B* **2011**, *115*, 5431–5440.

(26) Dinpajooh, M.; Matyushov, D. V. *J. Phys. Chem. B* **2014**, *118*, 7925–7936.

(27) Tanimura, Y.; Maruyama, Y. *J. Chem. Phys.* **1997**, *107*, 1779–1793.

(28) Toutounji, M. *Chem. Phys. Lett.* **2015**, *618*, 37–41.

(29) Toutounji, M. *Chem. Phys. Lett.* **2015**, *629*, 18–22.

(30) Beck, M. H.; Jäckle, A.; Worth, G. A.; Meyer, H.-D. *Phys. Rep.* **2000**, *324*, 1–105.

(31) Nest, M.; Meyer, H.-D. *J. Chem. Phys.* **2003**, *119*, 24–33.

(32) Cooley, J. W. *Math. Comp.* **1961**, *15*, 363–374.

(33) Yurchenko, S. N.; Thiel, W.; Jensen, P. *J. Mol. Spectrosc.* **2007**, *245*, 126–140.

(34) Bytautas, L.; Matsunaga, N.; Nagata, T.; Gordon, M. S.; Ruedenberg, K. *J. Chem. Phys.* **2007**, *127*, 204313.

(35) Bytautas, L.; Matsunaga, N.; Ruedenberg, K. *J. Chem. Phys.* **2010**, *132*, 074307.

(36) Bytautas, L.; Matsunaga, N.; Scuseria, G. E.; Ruedenberg, K. *J. Phys. Chem. A* **2011**, *116*, 1717–1729.

(37) Colbert, D. T.; Miller, W. H. *J. Chem. Phys.* **1992**, *96*, 1982–1991.

(38) Holstein, T. *Ann. Phys.* **1959**, *8*, 325–342.

(39) Crisp, M. D. *Phys. Rev. A* **1992**, *46*, 4138–4149.

(40) Silverstein, D. W.; Jensen, L. *J. Chem. Phys.* **2012**, *136*, 064111.

(41) Butkus, V.; Valkunas, L.; Abramavicius, D. *J. Chem. Phys.* **2012**, *137*, 044513.

(42) Butkus, V.; Zigmantas, D.; Abramavicius, D.; Valkunas, L. *Chem. Phys. Lett.* **2013**, *587*, 93–98.

(43) Bašinskaite, E.; Butkus, V.; Abramavicius, D.; Valkunas, L. *Photosynth. Res.* **2014**, *121*, 95–106.

(44) Duan, H.-G.; Nalbach, P.; Prokhorenko, V. I.; Mukamel, S.; Thorwart, M. *New J. Phys.* **2015**, *17*, 72002.

(45) Hsue, C.-S.; Chern, J. L. *Phys. Rev. D* **1984**, *29*, 643–647.

(46) Jafarpour, M.; Afshar, D. *J. Phys. A* **2002**, *35*, 87.

(47) Chung, N. N.; Chew, L. Y. *Phys. Rev. A* **2007**, *76*, 32113.

(48) May, V.; Kühn, O. *Charge and Energy Transfer Dynamics in Molecular Systems*; Wiley-VCH Verlag GmbH & Co. KGaA, 2011; pp 255–307.

(49) Valkunas, L.; Abramavicius, D.; Mančal, T. *Molecular Excitation Dynamics and Relaxation*; Wiley-VCH Verlag GmbH & Co. KGaA, 2013; pp 295–314.

(50) Mukamel, S. *Phys. Rev. A* **1983**, *28*, 3480–3492.

(51) Mukamel, S. *Principles of nonlinear optical spectroscopy*; Oxford University Press: New York; Oxford, 1999.

(52) Kubo, R. *J. Phys. Soc. Jpn.* **1962**, *17*, 1100–1120.

(53) Loan, C. V. *IEEE T. Automat. Contr.* **1978**, *23*, 395–404.

(54) Carbonell, F.; Jímenez, J. C.; Pedroso, L. M. *J. Comput. Appl. Math.* **2008**, *213*, 300–305.

(55) Higham, N. J. *SIAM J. Matrix Anal. Appl.* **2005**, *26*, 1179–1193.

(56) Al-Mohy, A. H.; Higham, N. J. *SIAM J. Matrix Anal. Appl.* **2009**, *31*, 970–989.

(57) Moler, C.; Van Loan, C. *SIAM Rev.* **2003**, *45*, 3–49.

(58) Dahl, J. P.; Springborg, M. *J. Chem. Phys.* **1988**, *88*, 4535–4547.

(59) Gallas, J. A. C. *Phys. Rev. A* **1980**, *21*, 1829–1834.

(60) Childs, D. R. *J. Quant. Spectrosc. Radiat. Transfer* **1964**, *4*, 283–290.

(61) de Lima, E. F.; Hornos, J. E. M. *J. Phys. B* **2005**, *38*, 815.

(62) Bytautas, L.; Matsunaga, N.; Nagata, T.; Gordon, M. S.; Ruedenberg, K. *J. Chem. Phys.* **2007**, *127*.

(63) Miyanaga, T.; Fujikawa, T. *J. Phys. Soc. Jpn.* **1998**, *67*, 2930–2937.

(64) Nitta, K.; Miyanaga, T.; Fujikawa, T. *J. Phys. Soc. Jpn.* **2006**, *75*, 54603.

(65) Chan, S. I.; Stelman, D.; Thompson, L. E. *J. Chem. Phys.* **1964**, *41*, 2828–2835.

(66) Seidner, L.; Domcke, W. *Chem. Phys.* **1994**, *186*, 27–40.

(67) Farag, M. H.; Jansen, T. L. C.; Knoester, J. *J. Phys. Chem. Lett.* **2016**, *7*, 3328–3334.

(68) Smith, P. J. *Am. Stat.* **1995**, *49*, 217–218.

(69) Plenio, M. B.; Almeida, J.; Huelga, S. F. *J. Chem. Phys.* **2013**, *139*.

(70) Jeske, J.; Ing, D. J.; Plenio, M. B.; Huelga, S. F.; Cole, J. H. *J. Chem. Phys.* **2015**, *142*.

(71) Crooks, G. E. *Phys. Rev. A* **2008**, *77*, 34101.

F Table of Contents Graphic